A Simulated Annealing Study of Diblock Copolymer Brushes in Selective Solvents

Yuhua Yin,[†] Pingchuan Sun,[‡] Baohui Li,*[,†] Tiehong Chen,[‡] Qinghua Jin,[†] Datong Ding,[†] and An-Chang Shi*[,†,§]

College of Physics, and the Key Laboratory of Functional Polymer Materials, Ministry of Education, and College of Chemistry, Nankai University, Tianjin, 300071, People's Republic of China, and Department of Physics and Astronomy, McMaster University, Hamilton, Ontario L8S 4M1, Canada

Received February 14, 2007; Revised Manuscript Received May 4, 2007

ABSTRACT: We report a simulated annealing study of the morphology of block copolymer brushes in selective solvents. The investigation is carried out with a lattice model, in which the ends of A-blocks of monodisperse linear AB diblock copolymer flexible chains are grafted regularly on a flat substrate plane with an equal "spacing". The morphological dependences of the brushes on solvent selectivity, polymer grafting density, and block lengths are investigated systematically. Phase diagrams of the system are constructed. Snapshots, polymer density profiles, and average contact numbers of the blocks are used to provide detailed information about the system. It is observed that multiple morphological transitions can be induced by varying block lengths as well as polymer grafting densities. At very low polymer grafting density, B-pinned or A-legged micelles or "flowerlike" structures are observed when the solvent is selective for the A or the B-blocks, respectively. Morphological transitions as well as size and spacing of the micellar aggregates can be manipulated by varying the block lengths. These predicted phase diagrams are consistent with available experiments and theories.

Introduction

Polymer brushes, composed of flexible polymer chains tethered to solid substrates, are a subject of intensive theoretical and experimental investigations.[1−7] Potential applications for polymer brushes include colloidal stabilization,[8] chemical gates,[9] drug delivery,[10] biomimetic materials,[11] modification of lubrication, friction, adhesion and wettability of surfaces,[12−14] and nanotechnology in transporting of adsorbed nanoparticles.[15,16] The tethered chains in polymer brushes can be homopolymers, mixtures of homopolymers, random copolymers, block copolymers, or functionalized polymers.

Brushes based on block copolymers[17−22] and mixed brushes[23−25] are particularly interesting because there are two factors affecting the behavior of the brushes. The polymer chains are covalently attached to a solid substrate. At the same time, the repulsive interaction between incompatible components drives the system to phase separation. The interplay of these two factors is expected to induce a large variety of surface morphologies. Furthermore, the presence of selective solvents was observed to cause significant conformational rearrangements.[26−28] Such a system possesses the property of changing the surface topography in response to different external conditions. This simple and yet very powerful method of tailoring surface topologies has led to exciting developments in utilizing surface-grafted polymers as potential "soft vehicles" capable of moving nanosized objects.[15,16] Besides linear block copolymer brushes in which polymers are tethered by one end to a solid surface, researches have also been carried out for Y-shaped brushes in which the copolymer is tethered to a solid surface through its junction point.[29−33] The morphology of block copolymer brushes depends on the particular points at which the macromolecule is attached.

Understanding the mechanism of structural formation in these brush systems would open some exciting possibilities to create structured surfaces with a controllable periodic pattern. These structured surfaces are expected to be of great interest for various applications. However, in contrast to the experimental works, theoretical and/or simulation studies of block copolymer brushes in selective solvents are less developed.[17−19]

In this study, we investigate the behavior of linear AB diblock copolymers tethered onto a planar surface in selective solvents. The morphological dependences of the brushes on solvent quality, polymer grafting density, and lengths of individual blocks were investigated systematically. A rich variety of morphologies and morphological transitions are observed. The density profiles and average contact number of the blocks were calculated. The simulation results are compared with previous experimental observations and theoretical predictions.

Model and Methods

Our simulations were based on the simulated annealing technique, which is a well-known procedure for obtaining ground states of complex systems.[34,35] The "single-site bond fluctuation" model on a simple cubic lattice (Carmesin and Kremer[36] and Larson[37]) was utilized in our simulations. Our previous studies on this model system have demonstrated that the simulated annealing is an efficient method for studying self-assembled block copolymer morphologies in solutions[38,39] and in confined environments.[40, 41] In the current study, the simulated annealing method is used to obtain morphologies of diblock copolymer brushes in selective solvents. The model and algorithm are reviewed briefly below, and a detailed description can be found elsewhere.[40]

We consider monodisperse linear AB diblock copolymer flexible chains. The ends of the A-blocks of these polymer chains are tethered onto a planar surface to form a polymer brush. The number of monomers on each blocks is N_A and N_B, respectively, thus the total number of monomers in each chain is $N = N_A + N_B$. The

* Authors to whom correspondence should be addressed. E-mail: baohui@nankai.edu.cn; shi@mcmaster.ca.
† College of Physics, Nankai University.
‡ Key Laboratory of Functional Polymer Materials, Ministry of Education, and College of Chemistry, Nankai University.
§ Department of Physics and Astronomy, McMaster University, Hamilton, Ontario L8S 4M1, Canada.

10.1021/ma070393n CCC: $37.00
Published on Web 06/14/2007

simulation system is embedded in a simple cubic lattice of volume $V = L_x \times L_y \times L_z$. A homogeneous, impenetrable surface (the wall) is introduced at $z = 0$. The copolymer chains are grafted on to the wall by the end of the A-block, that is, the first A- monomer in each chain is at the $z = 0$ plane. The wall sites cannot be occupied by other monomers except the first A-monomer. The distance between two neighboring grafted points is d, which is the "spacing" in both x and y directions. The grafting density is defined as $\sigma = 1/d^2$. The bond length of the polymers is set to be 1, $\sqrt{2}$,and$\sqrt{3}$ so that each site has 26 nearest-neighbor sites. The excluded volume effect is included in the model such that two or more monomers cannot occupy one lattice site at the same time. Periodic boundary conditions are adopted in the x and y directions and the dimensions are $L_x = L_y = 54$ if not specified, and L_z is much larger than the chain length N.

The starting configuration of the current study is generated by putting an array of copolymer chains onto the lattice. The polymer chains are parallel to the z-axis and all chains are in an extended conformation. Thus, the distance between two neighboring chains is d in either x or y direction. After the desired number of chains has been generated, the remaining empty sites were assigned to solvent molecules. Starting from this initial state, the ground state of the system is obtained by executing a set of Monte Carlo simulations at decreasing temperatures.[40] The energy of the system is the objective function in the simulated annealing. In our simulation we consider the 26 nearest-neighbor interactions only. There are five types of effective pair interactions in the system, block A and block B, block A and solvent, block B and solvent, block A and wall, and block B and wall. These are modeled by assigning an energy $E_{ij} = \epsilon_{ij} k_B T_{ref}$ to each nearest-neighbor pair of unlike components i and j, where i, j = A, B, S (solvent), and W (wall) and ϵ_{ij} is a reduced interaction energy; k_B is the Boltzmann constant; and T_{ref} is a reference temperature. Specifically, we assume $\epsilon_{AB} = 0.5$ in all cases, which ensures the immiscibility between the A- and B-monomers. When the solvent is selective for A-blocks, we set $\epsilon_{AS} = -1.0$ and $\epsilon_{BS} = 1.0$, whereas when the solvent is selective for B-blocks, we set $\epsilon_{AS} = 1.0$ and $\epsilon_{BS} = -1.0$. We also assume $\epsilon_{AW} = \epsilon_{BW} > 0$; i.e., neither block adsorbs on the wall. Furthermore, we assume $\epsilon_{ii} = 0$, with i = A, B, S, W.

We applied the usual annealing schedule with $T_j = \gamma T_{j-1}$, where T_j is the temperature used in the jth annealing step and γ is a scaling factor. The annealing was continued until the temperature reached a predetermined value (T_F). In our simulations, $\gamma = 0.9$, $T_1 = 50 T_{ref}$, and T reaches T_F ($=T_{60}$) after 60 annealing steps. One Monte Carlo step (MCS) is defined as the average time required for all the lattice sites to be visited in an attempted move. At each annealing step, 15000 MCS are performed. To examine the dependence of the final morphologies on the starting configuration, we performed simulations of 15000 MCS at an athermal state (where all $\epsilon_{ij} = 0$) before the usual procedure. Our results show that the final morphologies do not depend on the starting configurations.

Results and Discussion

The results on two typical cases are presented in this section. In the first case the solvent is selective to the A-blocks (grafted blocks), thus the B-blocks (top blocks) form collapsed chains. In the second case the solvent is selective to the B-blocks, so the A-blocks form collapsed chains. In each case, three grafting densities ($\sigma = 0.25$, 0.111 and 0.028) range from high to low are used. In each case for a given grafting density, we have investigated the influence of the block length on the morphology of the copolymer brushes.

Solvent Selective for the A-Blocks: $\epsilon_{AS} = -1.0$ and $\epsilon_{BS} = 1.0$. This set of parameters is chosen so that the grafted copolymers are exposed to a solvent that is good for the A-blocks and poor for the B-blocks. In this case, the soluble A-blocks are basically forming a stretched brush, whereas the insoluble B-blocks exhibit several distinct morphologies, depending on the grafting density and the lengths of the A- and B-blocks. The B-block structures are either on the top of or partly inside the A-brush.

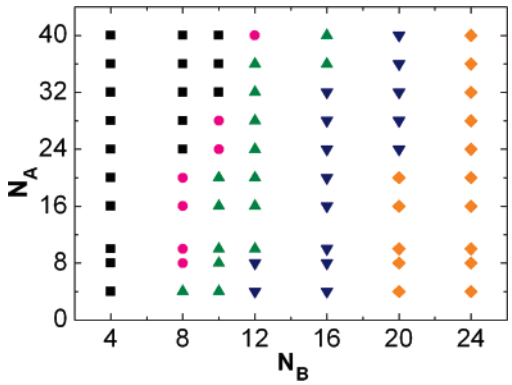

Figure 1. Phase diagram for systems with $\sigma = 0.25$ in the N_A and N_B space. The squares represent spherical structures; the circles, wormlike structures; the up triangles, ripple structures; the down triangles, perforated layer structures; and the diamonds, layer structures.

For the high grafting density at $\sigma = 0.25$, the morphologies of the B-blocks are summarized in the phase diagram shown in Figure 1, where different morphologies are represented by different symbols. It is interesting to notice that spherical structures are observed for smaller N_B, and layer structures are observed for larger N_B. However, for an intermediate value of N_B, there are morphological transitions with the increase of N_A. At $N_B = 8-10$, a morphological sequence from a ripple structure to a wormlike structure and then to an approximately hexagonally packed spherical structure are observed with the increase of N_A. At $N_B = 12$, 16, and 20, morphological sequences are from a perforated layer to a ripple and then to a wormlike structure; from a perforated layer to a ripple structure, and from a layer to a perforated layer structure, respectively, with the increase of N_A.

For the morphological sequence with $N_B = 10$, representative snapshots are plotted in Figure 2, where a ripple structure, a wormlike structure and a spherical structure are shown. From a detailed check of the chains, we noticed that the A-chains are highly stretched especially for copolymers with the smallest N_A. However, we also noticed that not all of the A-chains are perpendicular to the wall even for copolymers with the smallest N_A. Instead, most of the A-chains are tilted toward their respective B-domains to bring the B-chains together. It is interesting to notice that the average distance between two neighboring ripples is roughly equal in all ripple structures with $N_B = 10$, and it is more interesting to notice that the average distance between two neighboring features (ripple, worm, or sphere) in the simulated morphologies shown in Figure 2 is roughly equal in all three structures.

The density profiles of the B-monomers for morphologies with $N_B = 10$ along the Z-direction are shown in Figure 3. It is noticed that the peak value of the density is about 0.55−0.50 for a ripple structure and it is about 0.45 and 0.35 for a wormlike structure and for a spherical structure, respectively. The density profiles indicate that a ripple structure is composed of semicylinder B-domains when N_A is smaller ($N_A \leq 8$), whereas it is composed of B-cylinders when N_A is larger. In each density profile, the width at the half of the maximum height can be defined as the average height for the corresponding feature. The density profiles further indicate that the average height for each feature is roughly the same in all three structures.

Our predicted results can be compared with recent experiments of Prokhorova et al. and Santer et al. on poly(methyl methacrylate-*b*-glycidyl methacrylate) (PMMA−PGMA) and

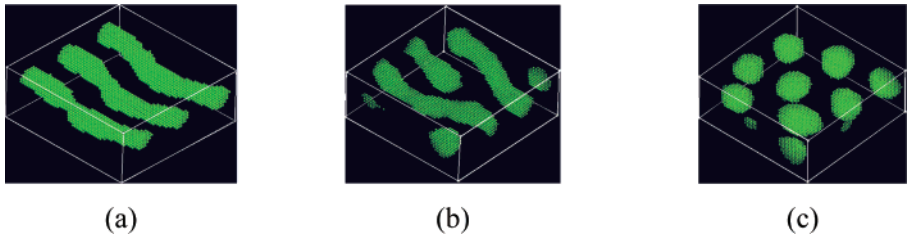

Figure 2. Typical morphologies of copolymer brushes as a function of N_A and $N_B = 10$ and $\sigma = 0.25$: (a) a ripple structure with $N_A = 20$; (b) a wormlike structure with $N_A = 28$; (c) a spherical structure with $N_A = 32$. Only B-monomers are shown.

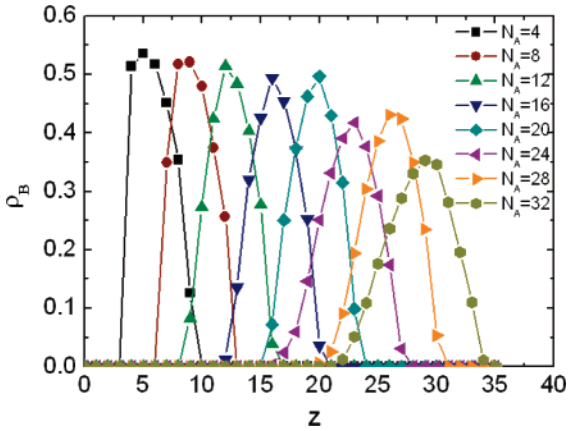

Figure 3. Density profiles of the B-monomers along the *Z*-direction for morphologies with $\sigma = 0.25$ and $N_B = 10$.

poly(benzyl-*n*-methacrylate-*b*-styrene) (p(BnMA-*b*-S)) brushes.[15,16] In their experiments, the solvent is selective to the grafted (PMMA in PMMA−PGMA and PBnMA in p(BnMA-*b*-S)) blocks, and poor to the top (PGMA in PMMA- PGMA and PS in p(BnMA-*b*-S)) blocks. For the PMMA−PGMA diblock copolymer brush, the degree of polymerization of the PMMA blocks changed from 600 to 700 and then to 800, while the degree of polymerization of the PGMA block was 308 in all three cases.[15] For the p(BnMA-*b*-S) diblock copolymer brush, the degree of polymerization of the PBnMA block changed from 500 to 800 and then to 1000, while the degree of polymerization of the PS block was kept at 400 in all three cases.[16] They observed morphological transitions from a ripplelike structure to a wormlike structure, and then to a spherical-like structure with the increase of the degree of polymerization of the grafted blocks in both copolymer brush systems, respectively. Our simulation results that morphological transitions from a ripple structure to a wormlike structure and then to a spherical structure can be induced by increasing N_A are in good agreement with these experimental observations.[15,16] Furthermore, in their experiments, Prokhorova et al. noticed that the height of the patterns and the distance between two neighboring features (ripple, worm or sphere) are similar in all three cases, i.e., 10 ± 1 nm in height and 50 ± 5 nm in distance, respectively for the PMMA−PGMA brush. Thus, our simulation results about the average height of the morphology and the average distance between two neighboring features are also in good agreement with these experimental observations.[15]

The density profiles of the A-blocks along the *Z*-direction are plotted in Figure 4a, in which the abscissa has been scaled by $(z + 1)/N_A$ for convenience. Figure 4a shows that for copolymers with the smallest N_A (=4), $\rho_A \approx \sigma$ in the whole region, whereas for copolymers with longer N_A, $\rho_A > \sigma$ for $(z + 1)/N_A < 0.7$ while ρ_A decreases sharply with the increase of $(z + 1)/N_A$ for $(z + 1)/N_A > 0.7$. These results indicate that the A-chains are fully stretched for copolymers with the shortest N_A and that they are less stretched for copolymers with longer N_A. For comparison, we have simulated the behavior of A-homopolymer brushes in good solvents. In the simulation, the length of the A-homopolymer is also varied from $N_A = 4$ to $N_A = 32$ with a step of 4 and with a grafting density of 0.25. The density profiles of the A-homopolymer brushes along the *Z*-direction are shown in Figure 4b. It is noticed that for the A-homopolymer brushes, $\rho_A \approx \sigma$ is always satisfied over the entire regions of $(z + 1)/N_A$ and for all chain lengths. This means that the A-homopolymer chains are fully stretched regardless of their length, which is the typical behavior of homopolymer brushes with high grafting density in good solvent. Comparing parts a and b of Figure 4, we can conclude that it is the existence of the insoluble B-blocks that is responsible for the lesser stretching of the A-blocks in block copolymer brushes.

The final morphology of a copolymer brush is the result of the competition between various interactions. The calculated average contact numbers for each A- and B-monomers as a function of N_A are shown in Figure 5, parts a and b, respectively. For a monomer that is far from the wall, its nearest-neighbors are one of the three species, i.e., the A-monomer, the B-monomer, and the solvent. The total contact number for each monomer should be the same as the number of nearest-neighbors, which is 26 in our model. However, for an A-monomer that is close to the wall, its nearest neighbors are one of the four species, i.e., the A-monomer, the B-monomer, the solvent, and the site in the wall. The total contact number for each such A-monomer should be slightly less than 26 due to the impenetrability of the wall. The average contact numbers for the A-monomer with B-monomers, solvents, and other A-monomers are defined as n_{AB}, n_{AS}, and n_{AA}, respectively. Similarly, the average contact numbers for the B-monomer with A-monomers and solvents are defined as n_{BA} and n_{BS}, respectively.

As shown in Figure 5a, n_{AS} increases while n_{AB} and n_{AA} decrease slightly with the increase of N_A. The relatively larger n_{AA} further indicates that not all of the A chains are perpendicular to the wall even for copolymers with the shortest N_A, otherwise, n_{AA} will be zero. On the other hand, Figure 5b shows that n_{BS} decreases while n_{BA} increases with the increase of N_A. It should be mentioned that the total number of A-monomers increases with the increase of N_A, while that of B-monomers is unchanged, which results in the different behaviors between n_{AB} and n_{BA}. As the B-blocks form collapsed chains, the domain formed by the B-monomers will be designated as the core, while the A-domain as the matrix. Thus, the quantity $n_{BA} + n_{BS}$ corresponds to the average contact of a B-monomer with other species. This quantity is proportional to the total surface area of the core and it is also plotted in Figure 5b. From this figure, it is clear that the total surface area of the core changes with the morphologies. Among the three structures, the spherical core has the smallest total surface area and the ripple core has the largest total surface area. As we know, the major contributions to the interaction energy of the system are from three parts as both components dewet the wall: the attractive interactions

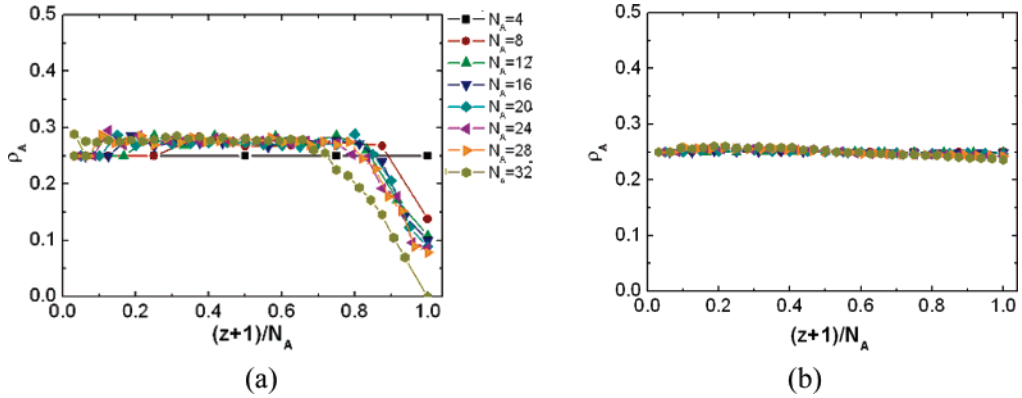

Figure 4. Density profile of the A-monomers along the *Z*-direction with $N_A = 4-32$, for (a) diblock copolymers with $N_B = 10$ and (b) A-homopolymers.

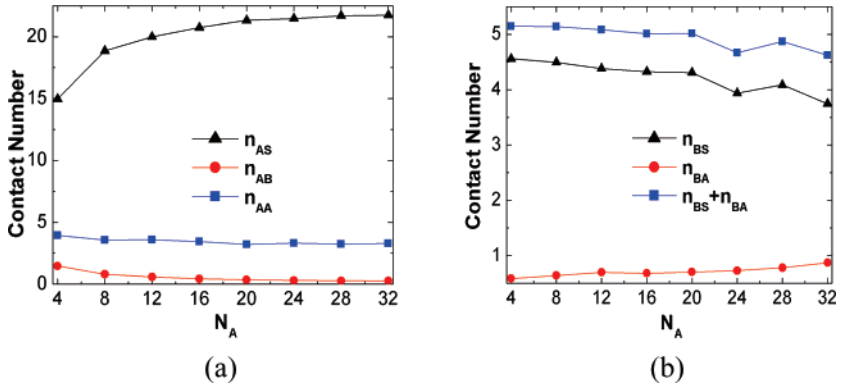

Figure 5. Variation of the average contact number with N_A for (a) A-monomer and (b) B-monomer.

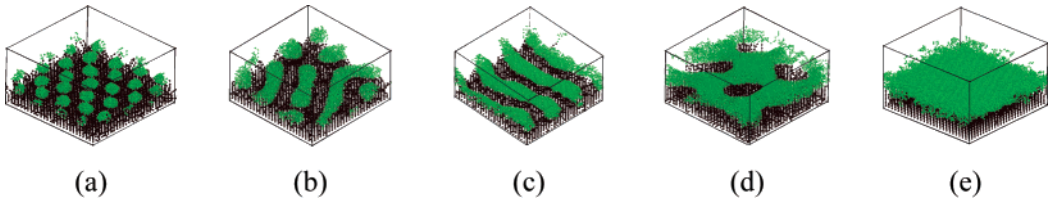

Figure 6. Morphologies of copolymer brush for different length of the B-block with $\sigma = 0.25$ and $N_A = 10$: (a) spherical micelles, $N_B = 4$; (b) wormlike micelles, $N_B = 8$; (c) stripe structure, $N_B = 10$; (d) perforated layer, $N_B = 16$; (e) layer, $N_B = 20$. In this and the following figures, the A-monomers are shown as dark areas and B-monomers are light areas.

between the A- monomers and the solvent molecules, the repulsive interactions between the B-monomers and the solvent molecules, and the repulsive interactions between the A- and B-monomers. So the contact of the A-monomers with the solvents is favorable, whereas the contact of the B-monomers with the solvents and that between the A- and B-monomers is unfavorable. In our model, $\epsilon_{BS} > \epsilon_{AB}$, which means the contact between the A- and B-monomers is preferred over that of the B-solvent. Thus, it results in the fact that n_{BS} decreases while n_{BA} increases with the increase of N_A in Figure 5b. On one hand, the increase in the A-B contact at such a high grafting density means that A-chains have to bend. That is, the A-blocks are bended to separate the contact between B-monomers and solvent molecules. On the other hand, the increase in the A−B contact can result in the decrease in the contact of A-solvent, and the latter is unfavorable in energy. Therefore, just as in other solution systems,[39] it is the competition between n_{AB}, n_{AS}, and n_{BS} that leads to the formation of different morphologies. Thus, the morphology of a block copolymer brush in solvent also depends on the values of ϵ_{AB}, ϵ_{AS}, and ϵ_{BS} besides the block lengths.

As shown in Figure 1, morphological transitions also occur with the increase of N_B. At a fixed N_A, a morphological sequence, spherical to wormlike structure to ripple structure to perforated layer structure and then to a layer structure, is always observed with the increase of N_B. However, the N_B region of spherical structures increases with N_A, and all the boundaries move to slightly larger N_B values with the increase of N_A. The representative snapshots for the morphologies with the increase of N_B are shown in Figure 6. Figure 6a is the morphology formed when $N_B = 4$, in which the B-monomers form a relatively regular hexagonally packed spherical pattern. Figure 6b shows the morphology formed when $N_B = 8$, which consists of wormlike B-domains. As N_B is increased to 10, a ripple structure is formed. As shown in Figure 6c, the ripple structure is actually consisting of cylindrical B-domains. When N_B is further increased to 16, the B-blocks form a layer but with some holes (see Figure 6d). This structure can be regarded as an inverted micelle. Since now the B-component is the majority species relative to the solvent molecule in the few effective layers, and the latter forms the holes in the continuous B-domain. When N_B is further increased to 20 and up, a B-layer is formed which covers the entire top surface of the A-brushes (see Figure 6e).

Figure 7 shows the density profiles of both the A- and B-monomers along the *Z*-direction for the morphologies shown

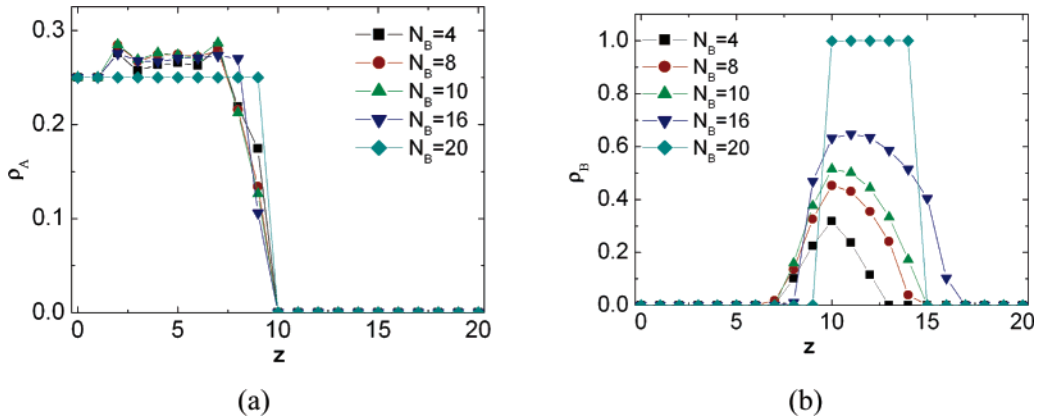

Figure 7. Density profiles of both the A- monomers (a) and the B-monomers (b) along the *Z*-direction for morphologies shown in Figure 6.

in Figure 6. From Figure 7a it is noticed that the density profiles of the A-monomers with $N_B = 4-16$ are similar to those plotted in Figure 4a. That is, $\rho_A > \sigma$ for the middle several layers while ρ_A decreases sharply in the top few layers. Whereas for copolymers with $N_B = 20$, $\rho_A = \sigma$ in the whole region. Thus, they indicate that the A-blocks are slightly bended when $N_B \leq 16$ whereas they are fully extended in a layer structure with $N_B = 20$. From Figure 7b it is noticed that the density curves are parabola-like when $N_B = 4-16$, and the peak values are about 0.3, 0.45, 0.50, and 0.65 for spherical, wormlike, ripple and perforated layer structures, respectively. The curve is steplike, and $\rho_B = 1$ for the layer structure with $N_B = 20$. These density curves are consistent with the morphologies shown Figure 6. They indicate that the average height for each feature (sphere, worm, ripple or perforated layer) in the simulated morphologies increases with N_B. Comparing the density profiles shown in Figure 3 and in Figure 7b, it is noticed that the peak values for the corresponding structures in the two cases are very similar. As the A-monomer is solvent-soluble while the B-monomer is solvent-insoluble, we take the B-monomer as one component while the A-monomer and solvent as another. It is noticed that the fraction of the B-monomer in the effective layers is approximately 50% in all ripple structures, while it is less than 30% in all spherical structures.

From Figure 1, we notice that similar morphological transitions can be induced either by increasing the length of the grafted block or by decreasing the length of the top block of the copolymer. It is also noticed that the morphologies are richer and more sensitive to the changes of N_B. The region of wormlike structures is very narrow in the phase diagram. A wormlike micelle may be just an intermediate state between a spherical micelle and a ripple. In the study of homopolymers grafted to a surface in bad solvents, Williams predicted that a similar morphology may occur to allow the coronal chains to stretch less.[4]

Our detail examinations of all the morphologies and the density profiles with $\sigma = 0.25$ show that the average distance between two neighboring features (ripple or sphere), and the average radius for each feature, increase with the increase of N_B and do not depend on N_A. Careful computations show that the average distance between two neighboring ripples is about $4.0R_{eeB}$ and that between two neighboring spheres is about $4.3R_{eeB}$, where R_{eeB} is the end-to-end distance of Gaussian chains with length of N_B. Our computations further show that the average radius is about $1.0R_{eeB}$ for each ripple, and it is about $1.3R_{eeB}$ for each sphere. Thus, all these quantities seem to be approximately proportional to R_{eeB} at this high grafting density.

When the grafting density is decreased to $\sigma = 0.111$, the morphologies of the B-blocks are summarized in the phase

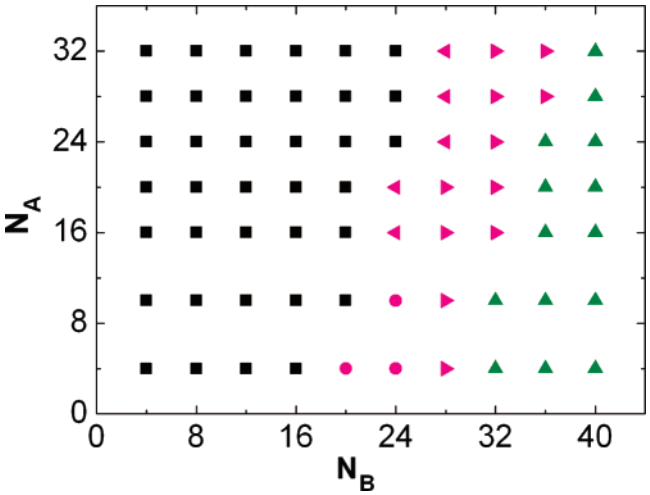

Figure 8. Phase diagram for systems with $\sigma = 0.111$ in the N_A and N_B coordinates, where the squares represent spherical structures; the circles, wormlike structures; the up triangles, ripple structures; the left and right triangles, degenerated structures of coexisting region I and II, respectively.

diagram shown in Figure 8. Similar to that shown in Figure 1, only spherical structures are observed for smaller N_B, and the N_B region of spherical structures enlarges with the increase of N_A. For a smaller N_A the typical morphological sequence with the increase of N_B is from a spherical structure to an ellipsoidal structure and then to a ripple structure, which is similar to that observed at high grafting density. However, there are differences between the phase diagrams with different grafting densities. One difference is that layer or perforated layer structures do not occur in the phase diagram with $\sigma = 0.111$ for the considered chain length range; instead, ripple structures are observed for larger N_B. Another difference is that there are two coexisting regions in the phase diagram with $\sigma = 0.111$ where two degenerated structures are always observed.

Figure 9 shows representative snapshots for the typical morphologies with the increase of N_B with $N_A = 10$. When $N_B = 4-20$, the B-blocks form approximately hexagonally packed spherical micelles. As N_B is increased to 24, the shape of the micelles becomes elongated or ellipsoidal or wormlike (Figure 9c). When N_B is further increased to 32, a ripple structure is formed (Figure 9d), which consists of parallel B-cylinders. From the side views of the structures, it is noticed that the A-blocks form a bigger boatlike corona wrapping around the bottom and sides of the B-cores in all cases.

Figure 10 shows the density profiles of the B-monomers along the direction perpendicular to the wall for the above morpho-

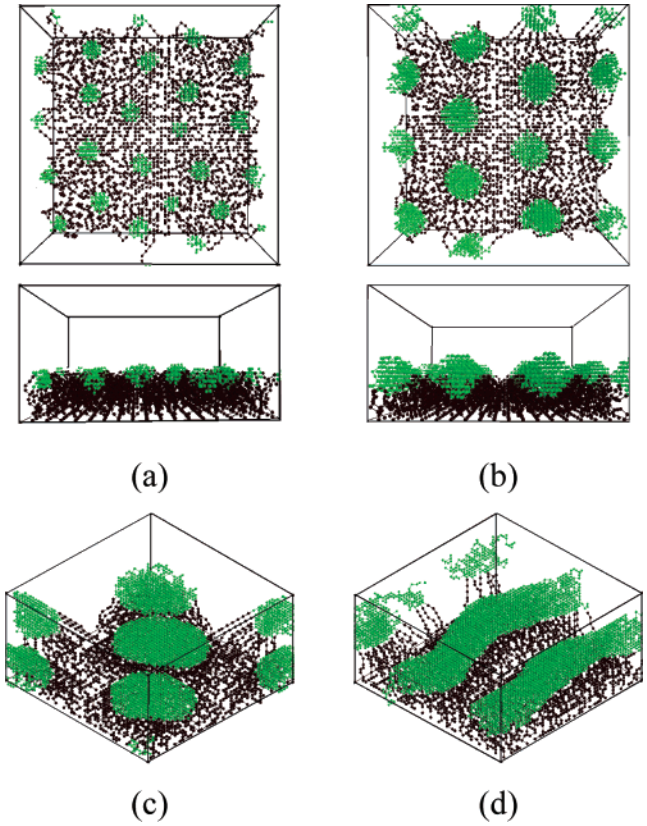

Figure 9. Morphologies of copolymer brush for different length of the B-block with $\sigma = 0.111$ and $N_A = 10$: (a) $N_B = 4$ and (b) $N_B = 12$, where the morphologies are viewed along two perpendicular directions; (c) $N_B = 24$ and (d) $N_B = 32$.

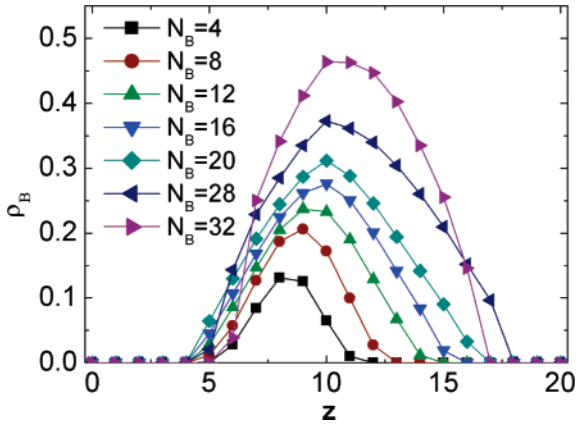

Figure 10. Density profile of the B-monomers along direction perpendicular to the wall for morphologies formed at the grafting density of $\sigma = 0.111$.

logical sequence with $N_A = 10$. It is noticed that the density curves are parabola-like for all the morphologies. The peak values in the density curves are about 0.1−0.3, 0.37, and 0.47 for spherical, wormlike, and ripple structures, respectively, which are slightly lower than the same values for the corresponding structures formed at high grafting density. Figure 10 further indicates that the average height for each feature (sphere, worm, or ripple) in the simulated morphologies also increases with N_B.

In contrast to the high grafting density case, we observed coexisting regions in this low grafting density case. Figure 11a shows the typical degenerated structures observed in the coexisting region I; one of them is a spherical structure and another is a mixed structure of spheres and ripples. Figure 11b shows the typical degenerated structures observed in the coexisting region II; one of them is a ripple structure and another is a mixed structure of wormlike micelles and ripples. These degenerated or mixed structures in coexisting regions may be a result of the fluctuations of the morphology at the boundary between the spherical and ripple structures at this low grafting density.

We further investigated the influence of N_A on the brush morphology at the grafting density of $\sigma = 0.111$. Figure 12 plotted the representative snapshots of the resulting morphologies as a function of N_A, where two sequences are given. As shown in Figure 12, spherical structures are formed when $N_B = 12$, and ripple structures are formed when $N_B = 32$ (the mixed structures are not shown here). There are no obvious differences in the size of the micelles and in the symmetry and the average distance between two neighboring features of the structures resulted from the same N_B but different N_A. However, it is noticed that, in the region of short N_A, the B-micellar cores are pinned close to the wall. As N_A increases, the A-blocks are incorporated into the "legs" of the micelles, the segments that tether the micellar core to the wall. With the further increase of N_A, the B-micellar cores become less laterally confined and a greater part of them are wrapped inside the A-brushes.

Figure 13 shows the density profiles of the B-monomers along the Z-direction for morphologies shown in Figure 12. It is noticed that the symmetric density curves are formed when $N_A \geq 10$. The peak values in the density curves are consistent with that plotted in Figure 10 and also slightly lower than that for the corresponding structures formed at high grafting density.

It is noticed that the average distance between two neighboring features (sphere or ripple) and the average radius for each feature in the simulated morphologies also increase with N_B at this low grafting density. Our computations show that the average distance between two neighboring ripples is in the range of $3.3-3.9R_{eeB}$ corresponding to N_B in the range of 30−40, and it is in the range of $3.7-4.1R_{eeB}$ between two neighboring spheres corresponding to N_B in the range of 10−28. That is, the increase of these average values with N_B is quick than that for R_{eeB}. Our computations further show that the average radius is about $0.8-0.9R_{eeB}$ for each ripple, and it is about $1.1-1.3R_{eeB}$ for each sphere.

The morphological transitions from a spherical to a wormlike and then to a ripple structure can also be induced through increasing N_B at the lower grafting density. However, the transition boundaries are moved to larger N_B values relative to those observed in the high grafting density case. This conclusion is reasonable considering that the number of the total chains decreases with the decrease of the grafting density. Thus, it is not surprising to notice that similar morphologies occur at about the same region in the phase diagrams whose coordinates are scaled in the $N_A\sigma$ and $N_B\sigma$. Furthermore, we can deduce that other morphological transitions, such as these to a perforated layer structure and to a layer structure observed in the high grafting density case can also occur at this lower grafting density provided N_B is larger enough. In contrast to the high grafting density case, we did not locate a morphological transition from a ripple structure and finally to a spherical one with the increase of N_A in the considered range in this low grafting density case. Our results indicate that such a morphological transition will occur at a larger N_A value in this low grafting density case if one exists.

These predicted results can be compared with previous experimental or theoretical results of block copolymer brushes. In the recent experiments of Tomlinson and co-workers, the

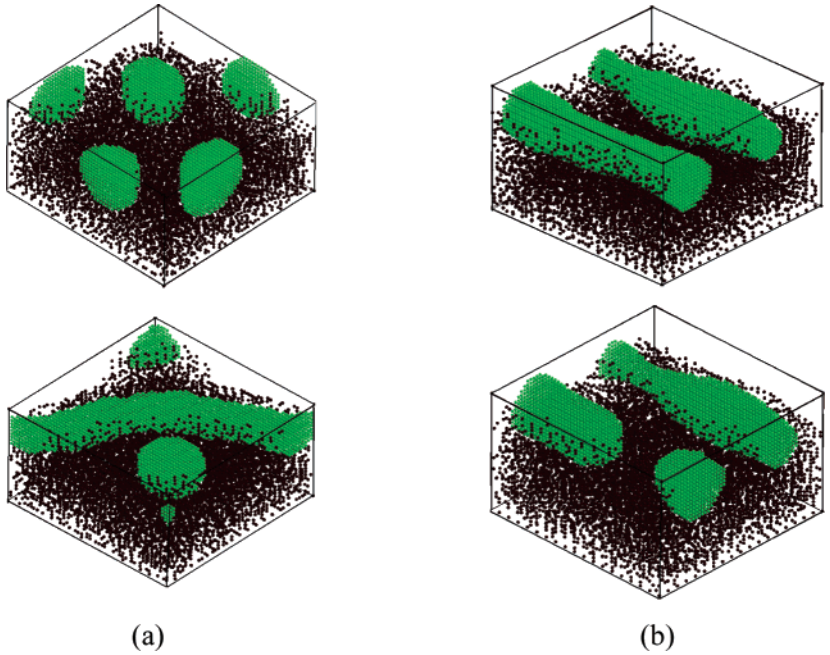

Figure 11. Degenerated structures formed with $N_A = 28$: (a) coexisting region I with $N_B = 28$ and (b) coexisting region II with $N_B = 36$.

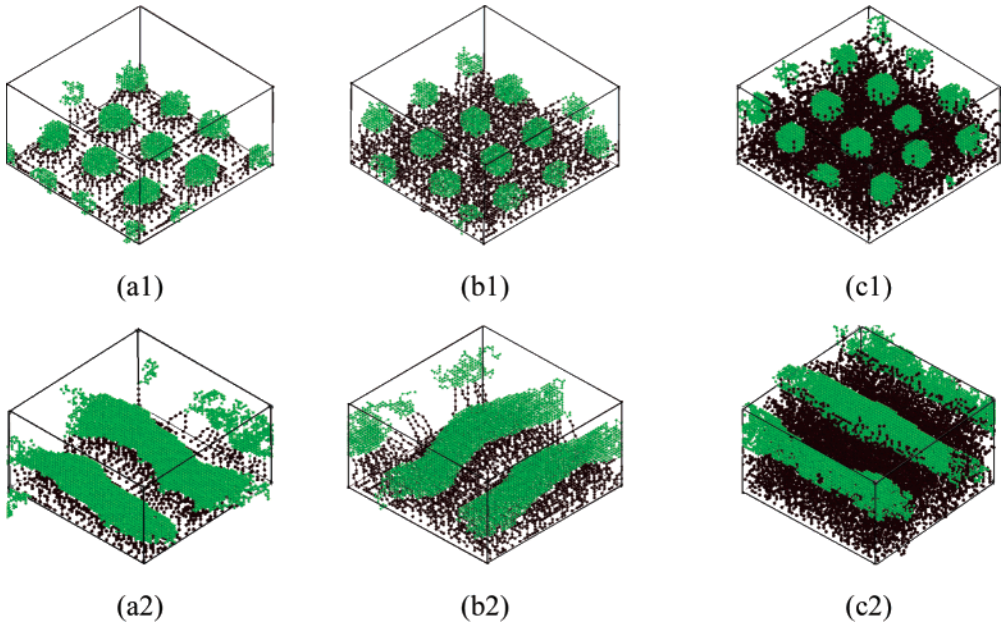

Figure 12. Typical morphologies of copolymer brushes as a function of N_A with $\sigma = 0.111$: (1) $N_B = 12$ and (a1−c1) $N_A = 4$, 10, and 20; (2) $N_B = 32$ and (a2−c2) $N_A = 5$, 10, and 32.

topography behavior of poly(2-hydroxyethyl methacrylate-*b*-methyl methacrylate) (PHEMA-*b*-PMMA) block copolymer brush was studied systematically as functions of both the PHEMA (grafted) and PMMA (top) block lengths, respectively, after selectively collapsing the top (PMMA) block.[28] Their results reveal that, in the region of short PHEMA, the PMMA micellar cores are pinned close to the surface. As the length of the PMMA block increases, the micellar cores increase in size; micelles are forced to approach one another, and they eventually form a bicontinuous honeycomb-like morphology. Moreover, the increase in size of the micelles is dependent primarily on the PMMA block length. Increasing the PHEMA block length dramatically enhances the lateral freedom of the micelles. Theoretically, Zhulina and co-workers studied the behavior of AB diblock copolymers more than a decade ago, where the copolymers are grafted to a planar surface in a solvent, that is a Θ solvent for the bottom block and a poor solvent for the top block, at relatively low densities.[17,18] Their self-consistent field calculations and scaling arguments predicted that the copolymer brushes exhibit several distinct morphologies: the regime of nonaggregating chains (I), A-legged micelles (MAB), pure B pinned micelles (PMB), the starlike block copolymer micelles (MA), and a bicontinuous phase (BAB). The morphological sequence from I to MAB or PMB and then to BAB is predicted with the increase of the top block length. While the morphological sequence from PMB to MAB and then to MA is predicted with the increase of the grafted block length. Our predicted results are in good agreement with these experimental and theoretical results.

When the grafting density is further decreased to $\sigma = 0.028$, the representative snapshots for the resulting morphologies are shown in Figure 14. As can be seen from this figure, only

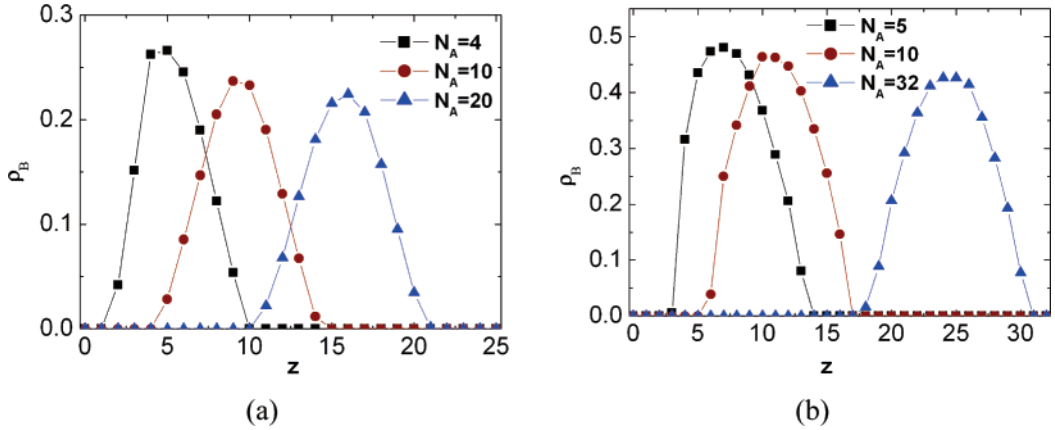

Figure 13. Density profiles of the B-monomers along the *Z*-direction for morphologies shown in Figure 12: (a) $N_B = 12$ and (b) $N_B = 32$.

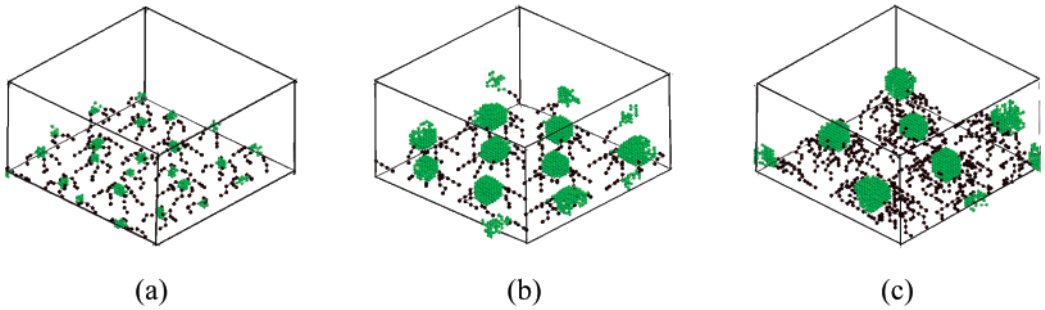

Figure 14. Morphologies of copolymer brush for different length of the A and B-blocks with $\sigma = 0.028$. (a) $N_A = 4$ and $N_B = 4$; (b) $N_A = 4$ and $N_B = 24$; (c) $N_A = 10$ and $N_B = 24$.

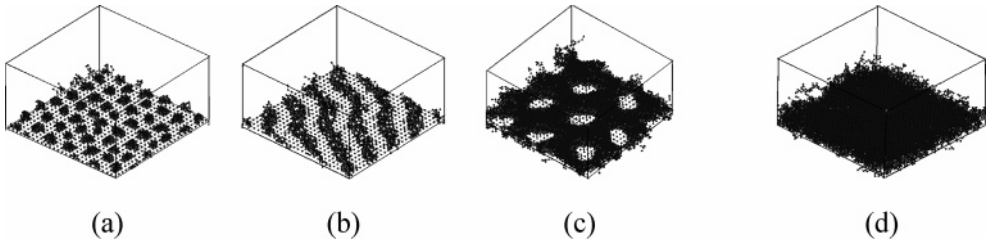

Figure 15. Morphologies of copolymer brushes for various N_A with $\sigma = 0.25$ and $N_B = 4$: (a) semispherical micelles with $N_A = 4$, (b) stripe structure with $N_A = 8$, (c) perforated layer with $N_A = 16$ and (d) layer with $N_A = 20$. Only the A-monomers are shown.

spherical micellar structure is formed in this case. With small N_A, the B-pinned or A-legged micelles are formed. With the increasing of either N_A or N_B, the size of the B-cores increases, and the number of micelles in the system decreases, which is different from that observed at the grafting density of $\sigma = 0.25$ or 0.111, where the size of the B-cores is dependent primarily on the N_B. It is also noticed that at smaller N_A, the A-blocks stretch in the lateral direction and the B-cores are confined near to the wall. With the increasing of N_A, the B-cores become less laterally confined and more free-floating in the top of the brushes. These predicted results are also consistent with the experimental observations of Tomlinson and co-workers and the theoretical predictions of Zhulina and co-workers mentioned earlier.[28,17,18]

Comparing the morphologies observed at the three grafting densities, we find that there exist morphological transitions induced through changing the grafting density. It is noticed that a spherical structure is always formed at a low grafting density (see Figure 14). In contrast, a ripple structure or a perforated layer or a layer structure can also be formed besides the spherical structure at a high grafting density (see Figures 1 and 8). Therefore, these results indicate that, depending on the structure at the high grafting density, a morphological transition from a ripple structure or from a perforated layer or from a layer structure to a finally spherical structure can be induced through decreasing the grafting density. This conclusion is also true for a symmetrical diblock copolymer. Similar morphologies and morphological transition were predicted by Minko et al.[26] and Müller[27] in the study of mixed brushes in solvents. They called the morphology of a spherical structure, in which the solvent-insoluble component forms clusters, as a "dimple" structure. They predicted a transition from a ripple structure to a "dimple" one for mixed brush of symmetrical composition when the quality of the solvent is changed from nonselective to selective for one component. All these results indicate that similar morphologies and morphological transition can be induced in both mixed brushes and block copolymer brushes.

Solvent Selective for the B-Blocks: $\epsilon_{AS} = 1.0$ and $\epsilon_{BS} = -1.0$. This set of parameters is chosen so that the grafted copolymers are exposed to a solvent that is good for the B-blocks and poor for the A-blocks. In this case, the insoluble A-blocks exhibit several distinct morphologies near the wall depending on their length, while the soluble B-blocks form brushes in the surface of the A-domains.

Figure 15 plotted the final morphologies obtained at a high grafting density ($\sigma = 0.25$), where we fix the length of the B-blocks at $N_B = 4$ and gradually increase the length of the A-blocks from 4 to 32 with a step of 4. It is noticed that with

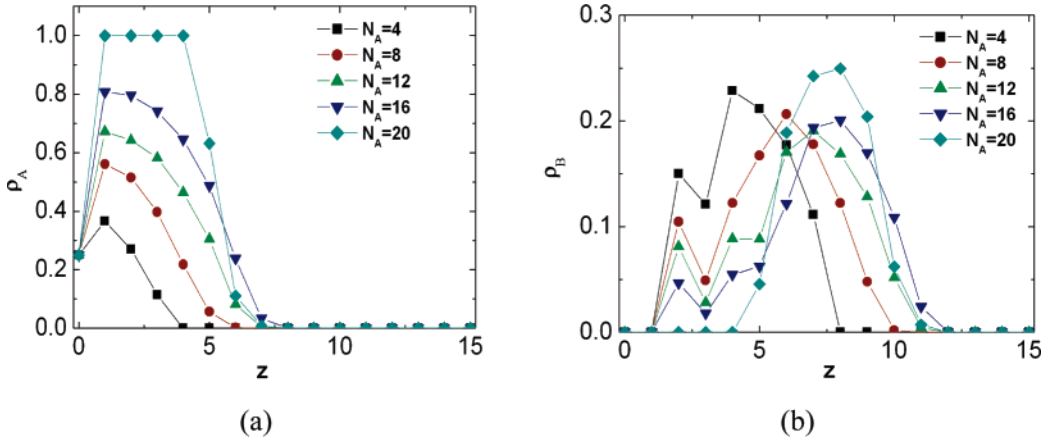

Figure 16. Density profiles along the *Z*-direction for morphologies shown in Figure 15 for (a) the A-monomers and (b) the B-monomers.

the increasing of N_A, the following morphological transitions take place for the A-domains: a semispherical structure (N_A = 4) to a ripple structure (N_A = 8−14) to a perforated layer (N_A = 16) and then to a layer ($N_A \geq 20$). This morphological sequence is very similar to that observed in the previous section for the B-blocks in the A-selective solvents (see Figure 6), which indicates that the solvent-insoluble blocks can form a similar morphological sequence when their length is changed whether they are grafted on the wall or on the top. Our further simulations indicate that the same trends as these for N_B = 4 can also be obtained with larger N_B.

The density profiles of both the A- and B-monomers along the *Z*-direction for morphologies with various N_A are plotted in Figure 16, parts a and b, respectively. In Figure 16a, it is noticed that the peak value of the curve increases with the increase of N_A, and it is 1 for the layer structure, which is consistent with the morphologies shown in Figure 15. It is also noticed that the peak values are slightly higher than those of the B-monomers for the corresponding structures obtained when the solvent is selective for the A- blocks. In Figure 16b, it is noticed that the density profiles of the B-monomers vary slightly with N_A, though the peak position occurs at a larger *z* value with the increase of N_A. One obvious feature of the density profiles is that the copolymer chains seemed to be confined to the several layers near to the wall. The A-chains are confined to the wall because a more stretched A-chain means greater contact of the A-solvent, which is unfavorable in terms of energy cost. The B-chains are also confined to near to the wall because the B-chains are always trying to separate the A-solvent contact. Our further simulations indicate that the chains do not have obvious stretch even for larger N_A or for larger polymer−wall interactions. It is also noticed that there is a small shoulder on the left of the main peak for each curve in Figure 16b with N_A <20. The small shoulder always occurs on the second layer above the wall, which is because that the strong B-wall interaction prevented the B-chains further down to near the wall.

For moderate and low grafting densities (σ = 0.111 and 0.028), only one type of structure is observed for the studied chain length (N_A= 4−32 and N_B = 4−32). The typical morphology is shown in Figure 17. This structure is just like a "flowerlike" structure where the core is formed by the insoluble A-blocks and the "petals" are formed by the soluble B-blocks. The size of the core increases with N_A, whereas it does not sensitive to N_B. This "flowerlike" structure was also predicted by Zhulina et al. in the case when the insoluble component of the diblock copolymers is grafted onto the planar surface.[18] In their case, the insoluble A-blocks form a dense micellar core while the soluble B-blocks form a shield around the B-micelles.

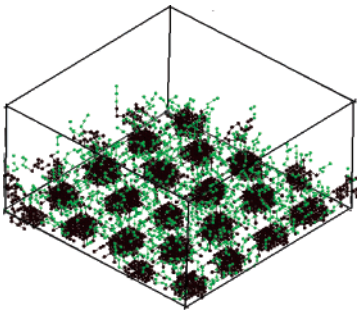

Figure 17. "Flowerlike" morphology of diblock copolymer brushes in selective solvent for B-blocks with N_A= 12, N_B = 4, and σ = 0.111.

Comparing the morphologies observed at the different grafting densities, we find that similar to the case of the A-selective solvents, there also exist morphological transitions induced through changing the grafting density.

It is noticed that the solvent-insoluble blocks can form a similar morphological sequence whether they are grafted on the wall or on the top when their length or the grafting density is changed. The predicted morphological transitions are in good agreement with available experiments and theories of block copolymer brushes. Recently, in the study of grafted homopolymers in a poor solvent with self-consistent field method as well as Monte Carlo simulations, Pattanayek and co-workers observed morphologies and morphological transitions similar to that predicted here, by either varying the grafting density or chain length.[42] It is also noticed that in some of our simulations with very short N_A or N_B, the chain conformations are stretched close to their maximal linear extension. This will lead to a loss of the configuration entropy and this situation may be quite different with that from experiments or self-consistent field theory.

Because the simulations were done in a finite box, it is expected that the packing of the patterns depends on the lateral size of the box. In order to test the influence of the lateral system size on the final morphology, simulations with different box sizes were performed. The results show that the lateral system size does not affect the final morphology. However, it does affect the packing of micelles in the final morphology. For example, spherical micelles with very regular hexagonal packing can be observed when the lateral system size matches the period of the micelles, whereas spherical micelles with approximately hexagonal packing can be observed when the lateral system size does not match the period of the micelles.

Conclusions

We used the simulated annealing method to obtain structures of AB diblock copolymers that are tethered onto a planar surface by the end of the A-blocks in selective solvents. The detailed morphology of a copolymer brush depends on the solvent selectivity, the grafting density, and the components of the copolymers. When the solvent is selective for the A-blocks, the A-blocks form a swelling brush, whereas the B-blocks form micelles in the top or partly inside of the A-brush. Phase diagrams for morphologies of the B-blocks are constructed. At high grafting density, morphological transitions from a ripple structure to a wormlike structure and then to a spherical structure, or from a perforated layer structure to a ripple structure, or from a layer to a perforated layer structure, depending on the length of the B-blocks, are predicted with increasing the length of the A-blocks. Similar morphological transitions can also be induced by decreasing the length of the B-blocks. At a relatively low grafting density, transitions similar to as that observed at high grafting density are observed. However, the same transitions occur at larger N_B values. At a very low polymer grafting density, B-pinned or A-legged micelles are observed. For most of our simulations, very similar morphologies are obtained for runs with different random number generator seeds. However, for system with grafting densities of 0.111, degenerated morphologies are observed near to the boundary between the spherical and ripple structures. When the solvent is selective for the B-blocks, at high grafting density, the following morphology transitions are observed with the increase of the length of the A-block: a semispherical structure to a ripple to a perforated layer and to a layer structure. At low grafting density, "flowerlike" structures are observed, where the A-blocks form collapsed micellar cores near to the wall, and the B-blocks form a shielding layer around the A-cores.

Morphological transitions similar to these induced through changing the block lengths can also be induced by changing the polymer grafting density. The predicted equilibrium morphologies and morphological transitions are in good agreement with available experiments and theories. It is hoped these predicted results can establish guidelines for tailoring the size and shape of the surface topologies and open the exciting possibility to design new surfaces with a controllable periodic pattern.

Acknowledgment. This research was supported by the National Natural Science Foundation of China (Grant Nos. 20474034, 20374031, and 20373029), by the Chinese Ministry of Education with the Program of New Century Excellent Talents in University and the Program of the Joint-Research Foundation of the Nankai and Tianjin Universities, and by Nankai University ISC. A.-C.S. acknowledges the support of the Natural Science and Engineering Council (NSERC) of Canada.

References and Notes

(1) Birstein, T. M.; Amoskov, V. M. *Polym. Sci.* **2000**, *C42*, 172.
(2) de Gennes, P. G. *Macromolecules* **1980**, *13*, 1069.
(3) Halperin, A.; Tirrell, M.; Lodge, T. P. *Adv. Polym. Sci.* **1992**, *100*, 31.
(4) Williams, D. R. M. *J. Phys. II* **1993**, *3*, 1313.
(5) Klein, J. *Annu. Rev. Mater. Sci.* **1996**, *26*, 581.
(6) (a) Julthongpiput, D.; LeMieux, M.; Tsukruk, V. V. *Polymer* **2003**, *44*, 4557. (b) Lemieux, M.; Minko, S.; Usov, D.; Stamm, M.; Tsukruk, V. V. *Langmuir* **2003**, *19*, 6126.
(7) (a) Singh, C.; Pickett, G. T.; Balazs, A. C. *Macromolecules* **1996**, *29*, 7559. (b) Singh, C.; Pickett, G. T.; Zhulina, B.; Balazs, A. C. *J. Phys. Chem. B* **1997**, *101*, 10614.
(8) Pincus, P. *Macromolecules* **1991**, *24*, 2912.
(9) Ito, Y.; Ochiai, Y.; Park, Y. S.; Imanishi, Y. *J. Am. Chem. Soc.* **1997**, *119*, 1619.
(10) Galaev, I.; Mattiasson, B. *Trends Biotechnol.* **1999**, *17*, 335.
(11) Aksay, A.; Trau, M.; Manne, S.; Honma, I.; Yao, N.; Zhou, L.; Fenter, F.; Eisenberger, P. M.; Gruner, S. M. *Science* **1996**, *273*, 892.
(12) Leger, L.; Raphael, E.; Hervert, H. *Adv. Polym. Sci.* **1999**, *138*, 185.
(13) Mansky, P.; Liu, Y.; Huang, E.; Russell, T. P.; Hawker, C. J. *Science* **1997**, *275*, 1458.
(14) Ruths, M.; Johannsmann, D.; Rühe, J.; Knoll, W. *Macromolecules* **2000**, *33*, 3860.
(15) Prokhorova, S. A.; Kopyshev, A.; Ramakrishnan, A.; Zhang, H.; Rühe, J. *Nanotechnology* **2003**, *14*, 1098.
(16) Santer, S.; Rühe, J. *Polymer* **2004**, *45*, 8279.
(17) Zhulina, E. B.; Singh, C.; Balazs, A. C. *Macromolecules* **1996**, *29*, 6338.
(18) Zhulina, E. B.; Singh, C.; Balazs, A. C. *Macromolecules* **1996**, *29*, 8254.
(19) Chern, S.-S.; Zhulina, E. B.; Pickett, G. T.; Balazs, A. C. *J. Chem. Phys.* **1998**, *108*, 5981.
(20) Zhao, B.; Brittain, W. J. *J. Am. Chem. Soc.* **1999**, *121*, 3557.
(21) Zhao, B.; Brittain, W. J.; Zhou, W.; Cheng, S. Z. D. *Macromolecules* **2000**, *33*, 8821.
(22) Kim, J.-B.; Huang, W.; Bruening, M. L.; Baker, G. L. *Macromolecules* **2002**, *35*, 5410.
(23) Minko, S.; Patil, S.; Datsyuk, V.; Simon, F.; Eichhorn, K.-J.; Motornov, M.; Usov, D.; Tokarev, I.; Stamm, M. *Langmuir* **2002**, *18*, 289.
(24) Lemieux, M.; Usov, D.; Minko, S.; Stamm, M.; Shulha, H.; Tsukruk, V. V. *Macromolecules* **2003**, *36*, 7244.
(25) LeMieux, M. C.; Julthongpiput, D.; Bergman, K. N.; Cuong, P. D.; Ahn, H.-S.; Lin, Y.-H.; Tsukruk, V. V. *Langmuir* **2004**, *20*, 10046.
(26) Minko, S.; Müller, M.; Usov, D.; Scholl, A.; Froeck, C.; Stamm, M. *Phys. Rev. Lett.* **2002**, *88*, 035502.
(27) Müller, M. *Phys. Rev. E* **2002**, *65*, 030802.
(28) Tomlinson, M. R.; Genzer, J. *Langmuir* **2005**, *21*, 11552.
(29) Julthongpiput, D.; Lin, Y.-H.; Teng, J.; Zubarev, E. R.; Tsukruk, V. V. *Langmuir* **2003**, *19*, 7832. Julthongpiput, D.; Lin, Y.-H.; Teng, J.; Zubarev, E. R.; Tsukruk, V. V. *J. Am. Chem. Soc.* **2003**, *125*, 15912.
(30) Zhulina, E. B.; Balazs, A. C. *Macromolecules* **1996**, *29*, 2667.
(31) Lin, Y.-H.; Teng, J.; Zubarev, E. R.; Shulha, H.; Tsukruk, V. V. *Nano. Lett.* **2005**, *5*, 491.
(32) LeMieux, M. C.; Lin, Y.-H.; Cuong, P. D.; Ahn, H.-S.; Zubarev, E. R.; Tsukruk, V. V. *Adv. Funct. Mater.* **2005**, *15*, 1529.
(33) Wang, Y.; Zheng, J. X.; Brittain, W. J.; Cheng, S. Z. D. *J. Polym. Sci., Part A: Polym. Chem.* **2006**, *44*, 5608.
(34) Kirkpatrick, S.; Gelatt, C. D.; Vecchi, M. P., Jr. *Science* **1983**, *220*, 671.
(35) Kirkpatrick, S. *J. Stat. Phys.* **1984**, *34*, 975.
(36) Carmesin, I.; Kremer, K. *Macromolecules* **1988**, *21*, 2819.
(37) Larson, R. G. *J. Chem. Phys.* **1992**, *96*, 7904; **1989**, *91*, 2479.
(38) Sun, P.; Yin, Y.; Li, B.; Chen, T.; Jin, Q.; Ding, D.; Shi, A.-C. *J. Chem. Phys.* **2005**, *122*, 204905.
(39) Yu, B.; Li, B.; Sun, P.; Chen, T.; Jin, Q.; Ding, D.; Shi, A.-C. *J. Chem. Phys.* **2005**, *123*, 234902.
(40) Yin, Y.; Sun, P.; Chen, T.; Li, B.; Jin, Q.; Ding, D.; Shi, A.-C. *ChemPhysChem.* **2004**, *5*, 540.
(41) Yu, B.; Sun, P.; Chen, T.; Jin, Q.; Ding, D.; Li, B.; Shi, A.-C. *Phys. Rev. Lett.* **2006**, *96*, 138306.
(42) Pattanayek, S. K.; Pham, T. T. *J. Chem. Phys.* **2005**, *122*, 214908.

MA070393N